Biosensors and Bioelectronics 212 (2022) 114420

Contents lists available at ScienceDirect

Biosensors and Bioelectronics

journal homepage: www.elsevier.com/locate/bios

Dual-emitting BP-CdTe QDs coupled with dual-function moderator TiO_2 NSs for electrochemiluminescence ratio bioassay

Jinwen Zhao [a], Yuting Zhou [a], Ying He [a], Xingrong Tan [b,**], Ruo Yuan [a], Shihong Chen [a,*]

[a] Key Laboratory of Luminescence Analysis and Molecular Sensing (Southwest University), Ministry of Education, College of Chemistry and Chemical Engineering, Southwest University, Chongqing, 400715, PR China
[b] Department of Endocrinology, 9 th People's Hospital of Chongqing, Chongqing, 400700, PR China

ARTICLE INFO

Keywords:
Electrochemiluminescence
TiO_2 nanosheets
CdTe QDs
Ratiometric assay
Alzheimer's disease

ABSTRACT

The limitation of the selection of dual-emitting luminophor and dual-function moderator makes the construction of single-luminophor-based electrochemiluminescence (ECL) ratio strategy extremely challenging. This work developed black phosphorus nanosheet loaded with CdTe quantum dots (BP-CdTe QDs) as dual-emitting luminophor, and TiO_2 nanosheets (NSs) as dual-function moderator to construct single-luminophor-based ECL ratio biosensor for amyloid-β protein (Aβ) detection. The BP-CdTe QDs modified glassy carbon electrode (GCE) firstly captured the anti-$A\beta_1$, and then the target Aβ. Finally, the secondary antibody composites containing *N*,*N*-diethylethylenediamine (DEDA) and TiO_2 NSs were captured on the electrode surface. DEDA in the secondary antibody composites and $S_2O_8^{2-}$ added in the detection solution served as the anodic and cathodic co-reactants, respectively, and TiO_2 NSs as co-reaction accelerator can simultaneously enhance two emissions. The increase of target concentration made the two signals show different increasing trend, thus achieving a sensitive ratio detection of target Aβ with the detection limit of 21 fg/mL. The dual-emitting BP-CdTe QDs coupled with dual-function moderator TiO_2 NSs provide an attractive single-luminophor-based ECL ratio platform for bioassay, which can not only be applied to the detection of Aβ, but also to the detection of other disease biomarkers.

1. Introduction

The ratio electrochemiluminescence (ECL) analysis based on two signal modes can eliminate the interference of instrument and environmental factors, so it has high accuracy and has been widely concerned in the environmental, food, drug and clinical detection (Huo et al., 2019; Zhang et al., 2020). Among, the single-luminophor-based ECL ratio strategy, in which the double signals come from the same luminophor rather than two different ones, has aroused great interest because it avoids the complexity of matching two luminophors and their co-reactant involved in dual-luminophor-based ratiometric strategy (Chen et al., 2016). However, its construction still faces great challenges due to the limitation of the selection of dual-emitting luminophor and dual-function moderator. Currently, only several dual-emitting luminophors were developed, including ruthenium (II) tris (2, 2′-bipyridyl) ($Ru(bpy)_3^{2+}$) (Cao et al., 2020), luminol (Shang et al., 2020), graphene quantum dots (Chen et al., 2019) and graphene carbon nitride quantum dots (Shang et al., 2015). The reported dual-emitting luminophors required special targets to achieve different change trends of two emissions, thus the practical application was limited. Developing a new type of dual-emitting luminophor which is not limited to the different variations of the dual signals triggered by a specific target is of great value.

For ECL ratio analysis, it is urgent to adopt dual-function moderators to mediate the different trends of two signals (He et al., 2021). The main dual-function moderators currently used were noble metal nanoparticles (NPs). Additionally, Hg^{2+}, H_2O_2 and G-quadruplex/hemin have also been reported as the dual-function moderators. For example, Au NPs and Pt NPs were respectively reported as the dual-function moderators to mediate the opposite changes of two emissions from luminol and graphene quantum dots (QDs) (Lei et al., 2015) and from luminol and CdS QDs (Zhang et al., 2013). Those reported noble metal nanoparticles usually achieve the changes of two signals by means of resonance energy transfer (RET) and their applications were limited by the distance dependence of RET. Our group recently developed H_2O_2 as dual-function moderator to regulate the dual emissions for in ratio

** Corresponding author.
* Corresponding author.
E-mail addresses: tanxingrong@yahoo.com (X. Tan), cshong@swu.edu.cn (S. Chen).

https://doi.org/10.1016/j.bios.2022.114420
Received 23 February 2022; Received in revised form 7 May 2022; Accepted 22 May 2022
Available online 24 May 2022

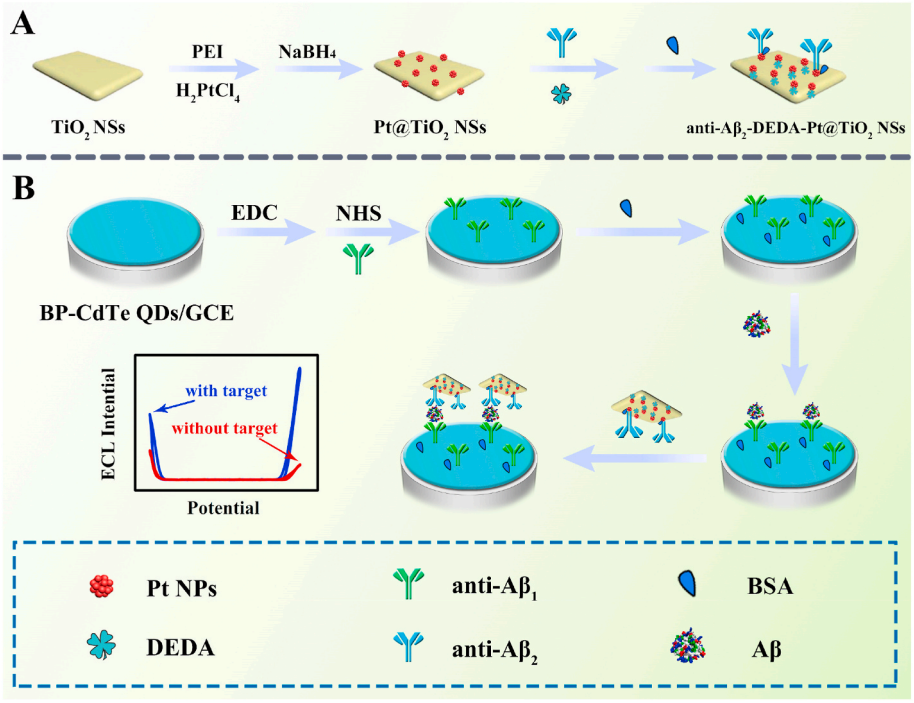

Scheme 1. (A) Preparation of anti-Aβ$_2$-DEDA-Pt@TiO$_2$ NSs; (B) fabrication of the biosensor for Aβ detection.

analysis (Yang et al., 2021), and it would undergo in suit production by enzyme-catalyzed reactions, thus limiting its application. As for G-quadruplex/hemin as dual-function moderator, its formation involved the application of DNAzyme and complex labeling processes (Wang et al., 2018). For Hg^{2+} as dual-function moderator (Wang et al., 2020), its application was restricted to the irreplaceability of Hg^{2+} as the target and the adverse effects of Hg^{2+} on the environment and organism. All of these dual-function moderators reported have their own limitations. Therefore, developing a RET-free, enzyme-free, labeling-free, and environmental-friendly dual-function moderator is of great significance for ECL ratio analysis.

The co-reaction accelerators, which can interact with the co-reactants to enhance ECL emission, have attracted much attention in ECL field (Hu et al., 2020; Wang, 2021). Common co-reaction accelerators include noble metal nanoparticles (Zhou et al., 2020), metal organic framework (MOF) (Wang et al., 2019a), transition metal oxides (Du et al., 2020) and small molecules such as hemin (Zeng et al., 2018), etc., which are generally used for a single signal enhancement (Hu et al., 2020). To date, it has not been reported that a single co-reaction accelerator can be used to enhance both the cathodic and anodic ECL emissions to construct ratio analysis. In fact, even the use of co-reaction accelerators to enhance one signal is rarely reported in ratio detection, only MOF (Wang et al., 2019b) and C_{60} (Lu et al., 2020) for accelerating the ECL emission of $Ru(bpy)_3^{2+}$ and O_2, respectively, which all used $S_2O_8^{2-}$ as co-reactant. Obviously, if a single co-reaction accelerator can simultaneously enhance two emissions in ratio analysis, it can not only improve the detection sensitivity, but also simplify the construction of the ratio strategy, and is a very attractive dual-function moderator. Among the co-reaction accelerators reported, TiO_2 nanosheets (TiO_2 NSs) have been studied extensively due to their excellent photoelectric performance, high specific surface area, high stability and environmental friendliness (Yu et al., 2021). Since it was reported that TiO_2 NSs could not only serve as co-reaction accelerator for amplifying the anodic signal with amine as co-reactant (Hao et al., 2021), but also could increase the cathodic ECL emission with $S_2O_8^{2-}$ as co-reactant (Ma et al., 2021), they have the potential to serve as the dual-function moderator in ratio sensing to simultaneously modulate two ECL emissions.

Due to stable light emission and high quantum yield, CdTe QDs are not only widely used in single signal ECL detection, but also used as the cathodic luminophor to construct dual-luminophor-based ECL ratio strategy (Gao et al., 2020; Pan et al., 2019). Although its unique cathodic and anodic emission properties show great application potential in single-luminophor-based ratiometric ECL strategy, few studies have been carried out. Our group applied black phosphorus (BP) for the first time to modulate the dual emissions of CdTe QDs and further combined dual-function moderator H_2O_2 to achieve single-luminophor-based ratiometric ECL detection (Zhao et al., 2021). In this strategy, H_2O_2 was produced in situ by enzyme-catalyzed reactions, and the unstable properties of H_2O_2 and the insufficiency of application enzymes cannot be ignored. Clearly, developing dual-function moderators that are not limited to enzyme system is necessary to extend the application of BP-CdTe QDs.

In view of above observations, a single-luminophor-based ECL ratio system was fabricated using dual-emitting BP-CdTe QDs as luminophor and TiO_2 NSs as dual-function moderator. Since the amyloid-β proteins (Aβ) was the crucial therapeutic target and diagnostic biomarker for Alzheimer's disease (Xue et al., 2019), and it was chosen as the target to build the sandwich immunosensor in this work. As shown in Scheme 1A, Pt NPs were grown in situ on the prepared TiO_2 NSs to covalently bond with N, N-diethylethylenediamine (DEDA) and anti-Aβ$_2$ for preparing the secondary antibody composite (anti-Aβ$_2$-DEDA-Pt@TiO_2 NSs) through the Pt-N bond. Meanwhile, BP-CdTe QDs with carboxyl groups were prepared for the modification of glassy carbon electrodes (GCE) and as the matrix for immobilizing anti-Aβ$_1$. With the incubation of the target Aβ, anti-Aβ$_2$-DEDA-Pt@TiO_2 NSs was captured on the GCE to form the sandwich structure (Scheme 1B). DEDA in the secondary antibody complex and $S_2O_8^{2-}$ added in the detection solution served as the anodic and cathodic co-reactants, respectively. TiO_2 NSs as co-reaction accelerator can simultaneously enhance two emissions. Due to the different increasing trends of two ECL signals, a highly sensitive ECL ratio detection of Aβ was realized. The dual-emitting BP-CdTe QDs coupled with dual-function moderator TiO_2 NSs provided a single-luminophor-based ratiometric ECL platform, showing a significant application prospects in the detection of Aβ or other disease

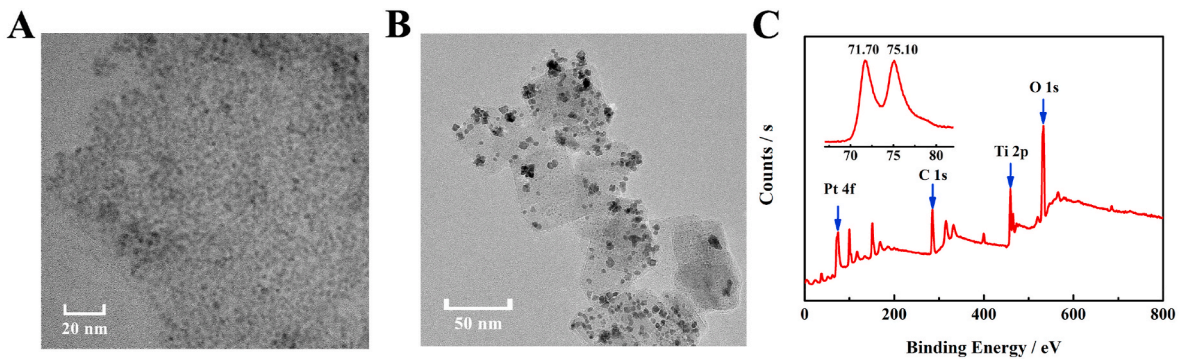

Fig. 1. TEM images of (A) BP-CdTe QDs and (B) Pt@TiO_2 NSs; XPS spectra of the full region of (C) Pt@TiO_2 NSs (insets: the enlarged curves of Pt).

biomarkers.

2. Experimental sections

2.1. Reagents, materials and instruments

Reagents, materials, and instruments applied in this work are presented in the Supplementary Material.

2.2. Preparation of Pt@TiO_2 NSs

The following method was applied to prepare TiO_2 NSs (Xie et al., 2020). Firstly, tetrabutyl titanate (20 mL) and hydrofluoric acid (2.4 mL) were added to a 150 mL Teflon autoclave and reacted at 180 °C for 24 h. The resulting white precipitate was collected by centrifuging at 12, 000 rpm and washed with ethanol and ultrapure water, and further dried in the oven for 12 h at 80 °C to obtain TiO_2 NSs powder.

TiO_2 NSs powder was dispersed in ultrapure water to produce its dispersion (0.5 mg/mL), which was used to synthesize Pt@TiO_2 NSs by following method. Firstly, the amino-rich polyethyleneimine (PEI) (3.0 mL 1%) was injected into TiO_2 NSs dispersion (3.0 mL, 1.0 mg/mL) and kept stirring for 1 h. Afterward, 500 μL of $HPtCl_4$ solution (1%) and 100 μL $NaBH_4$ solution (3.0 mM) were added slowly (Scheme 1A). With stirring for 6 h, the reaction products were collected by centrifugation for 10 min at 12,000 rpm and washed with ultrapure water. During in situ reduction of $HPtCl_4$ on TiO_2 NSs surface, the amino groups of PEI on the surface of TiO_2 NSs would provide a large number of binding sites for stably anchoring Pt NPs through the strong Pt-N bond. The as-prepared Pt@TiO_2 NSs were dispersed in 6.0 mL ultrapure water.

2.3. Preparation of anti-Aβ$_2$-DEDA-Pt@TiO_2 NSs

DEDA (10 μL), anti-Aβ$_2$ (50 μL, 10 μg/mL) and Pt@TiO_2 NSs dispersion (100 μL, 0.5 mg/mL) were added in 400 μL PBS (0.10 M, pH 7.4), and kept stirring at 4 °C for 14 h so that DAEA and anti-Aβ$_2$ were combined to the surface of Pt@TiO_2 NSs through Pt-N bonds. After the nonspecific binding sites of Pt NPs' surfaces were blocked using 50 μL of bovine serum albumin (BSA, 1%), the secondary antibody composites anti-Aβ$_2$-DEDA-Pt@TiO_2 NSs were obtained.

2.4. Preparation of BP-CdTe QDs

According to our previous work (Zhao et al., 2021), bulk BP was used to prepare BP nanosheet, which was further used to prepare BP-CdTe QDs. The details for BP-CdTe QDs preparation were as follows. 36.89 mg of $CdCl_2{\cdot}2.5H_2O$ was solved in ultrapure water (50 mL) to obtain its solution, which was mixed with BP nanosheet dispersion (1.0 mL). The resultant mixture was kept stirring for 1 h so that Cd^{2+} was adsorbed on the surface of BP nanosheet. Afterward, 0.010 M Na_2TeO_3 (1.0 mL), 3-mercaptopropionic acid (33 μL), $C_6H_5Na_3O_7{\cdot}2H_2O$ (50 mg) and $NaBH_4$ (0.1 g) were successively added. The resultant mixed solution was kept refluxing for 8 h at 130 °C so that CdTe QDs were grown on BP nanosheet. The produced precipitate was centrifuged (12000 rpm, 5 min), followed by washing with ethanol for three times. 5.0 mL of ultrapure water was used to disperse the collected BP-CdTe QDs.

2.5. Fabrication of ECL immunosensor

The assembly of immunosensor is depicted in Scheme 1B. Firstly, BP-CdTe QDs dispersion (10 μL) prepared above and 0.5% nafion (5.0 μL) were dripped onto the GCE ($\Phi = 4$ mm) surface, which was pre-polished referring to the literature (Yang et al., 2021). After being dried naturally in an air atmosphere, the modified GCE was treated with EDC/NHS solution in molar ratio of 4:1 for assembling the anti-Aβ$_1$ (10 μL,10 μg/mL) at 4 °C, and further incubated with BSA (1%) at 4 °C for 1 h so that nonspecific binding sites on GCE surface were blocked. The resultant immunosensor (anti-Aβ$_1$-BP-CdTe QDs/GCE) was stored at 4 °C for future use. The washing operation was performed using pH 7.4 PBS (0.10 M) for each modification step during assembly.

2.6. ECL measurement

The constructed anti-Aβ$_1$-BP-CdTe QDs/GCE was incubated with the target Aβ for 2 h, and further incubated with anti-Aβ$_2$-DEDA-Pt@TiO_2 NSs (15 μL) for 2 h. After the sandwich immune structure was formed at the biosensor, the ECL detection was performed in 0.10 M PBS (3.0 mL, pH 7.4) containing $K_2S_2O_8$ (5.0 mM) under the scanning potential of −1.5 V ~ +1.2 V, the scanning rate of 300 mV/s, and the voltage of 800 V for the photomultiplier.

3. Results and discussion

3.1. Characterization of nanomaterials

The as-prepared BP-CdTe QDs and Pt@TiO_2 NSs were analyzed by the TEM to investigate their morphologies. As seen from the TEM image of BP-CdTe QDs (Fig. 1A), a large number of CdTe QDs were evenly distributed on the surface of TiO_2 NSs, which is consistent with the previous work (Zhao et al., 2021). Fig. 1B depicts the TEM image of Pt@TiO_2 NSs. Obvious lamellar structures were observed and their surfaces were covered with a large number of Pt NPs. The Pt@TiO_2 NSs were further analyzed by XPS to characterize the chemical composition, and Fig. 1C illustrates the results. As seen, the characteristic peaks of C 1s, Ti 2p and O 1s were detected at 285.10 eV, 458.55 eV and 530.20 eV, respectively. Meanwhile, the characteristic peaks at 71.70 eV and 75.10 eV for Pt 4f were detected, demonstrating the preparation of Pt@TiO_2 NSs.

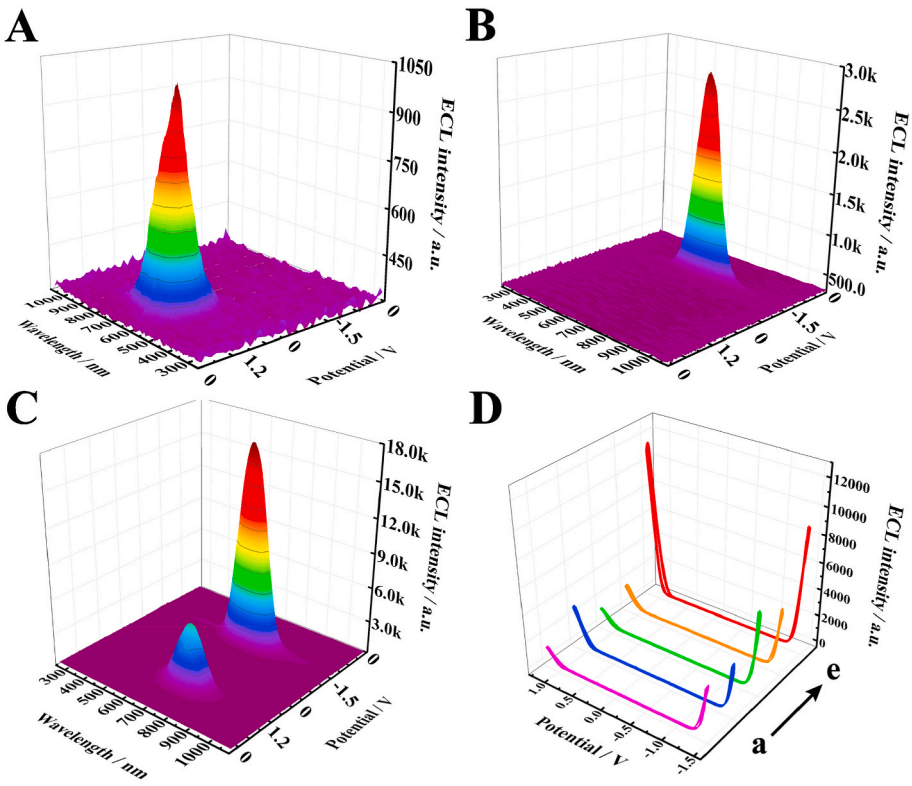

Fig. 2. ECL spectra of (A) BP nanosheet, (B) CdTe QDs and (C) BP-CdTe QDs modified GCE in 0.10 M PBS (pH 7.4) containing 10 mM DEDA and 10 mM $K_2S_2O_8$. (D) ECL response of BP-CdTe QDs/GCE in 0.10 M PBS (pH 7.4) without DEDA and $K_2S_2O_8$ (a), with 5.0 mM DEDA alone (b), with 5.0 mM $K_2S_2O_8$ alone (c), TiO_2 NSs/BP-CdTe QDs/GCE without (d) and with 5.0 mM $K_2S_2O_8$ and 5.0 mM DEDA (e).

3.2. ECL mechanism of immunoassay

To demonstrate the ECL emission mechanism of BP-CdTe QDs, three-dimensional (3D) ECL spectra of BP-CdTe QDs, CdTe QDs and BP nanosheet were investigated in the presence of DEDA (10 mM) and $K_2S_2O_8$ (10 mM) in PBS (0.10 M, pH 7.4). A weak anodic ECL emission with the maximum wavelength of 642 nm at +1.2 V was detected for BP nanosheet/GCE (Fig. 2A). As seen from Fig. 2B, the 3D ECL spectrum revealed a cathodic ECL emission with the maximum wavelength of 701 nm at −1.5 V, and no significant anodic emission was detected for CdTe QDs/GCE. However, both the anodic and cathodic ECL emissions were detected at +1.2 V and −1.5 V for BP-CdTe QDs/GCE (Fig. 2C),

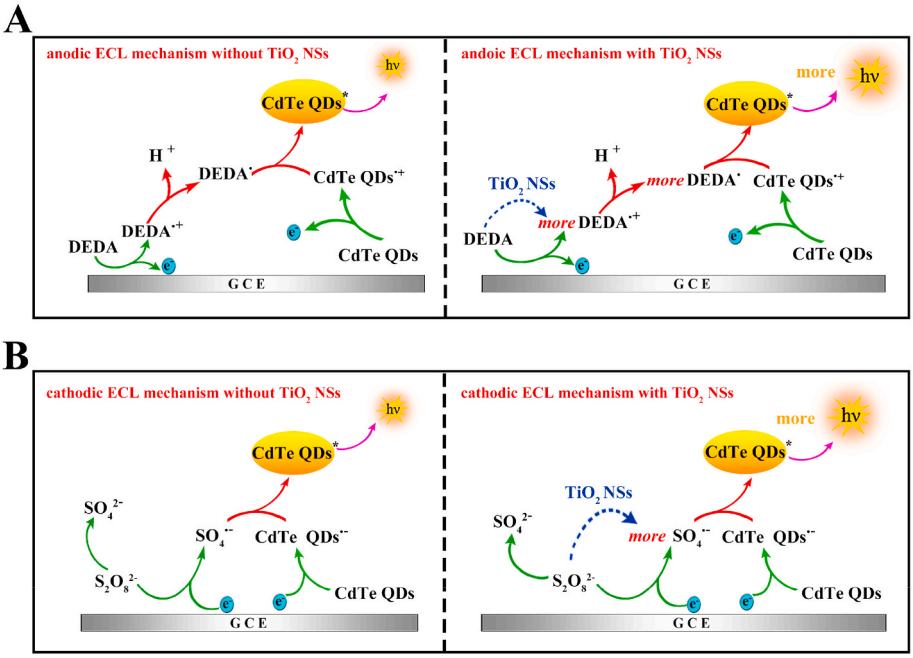

Fig. 3. ECL mechanisms of (A) anodic and (B) cathodic emissions of BP-CdTe QDs.

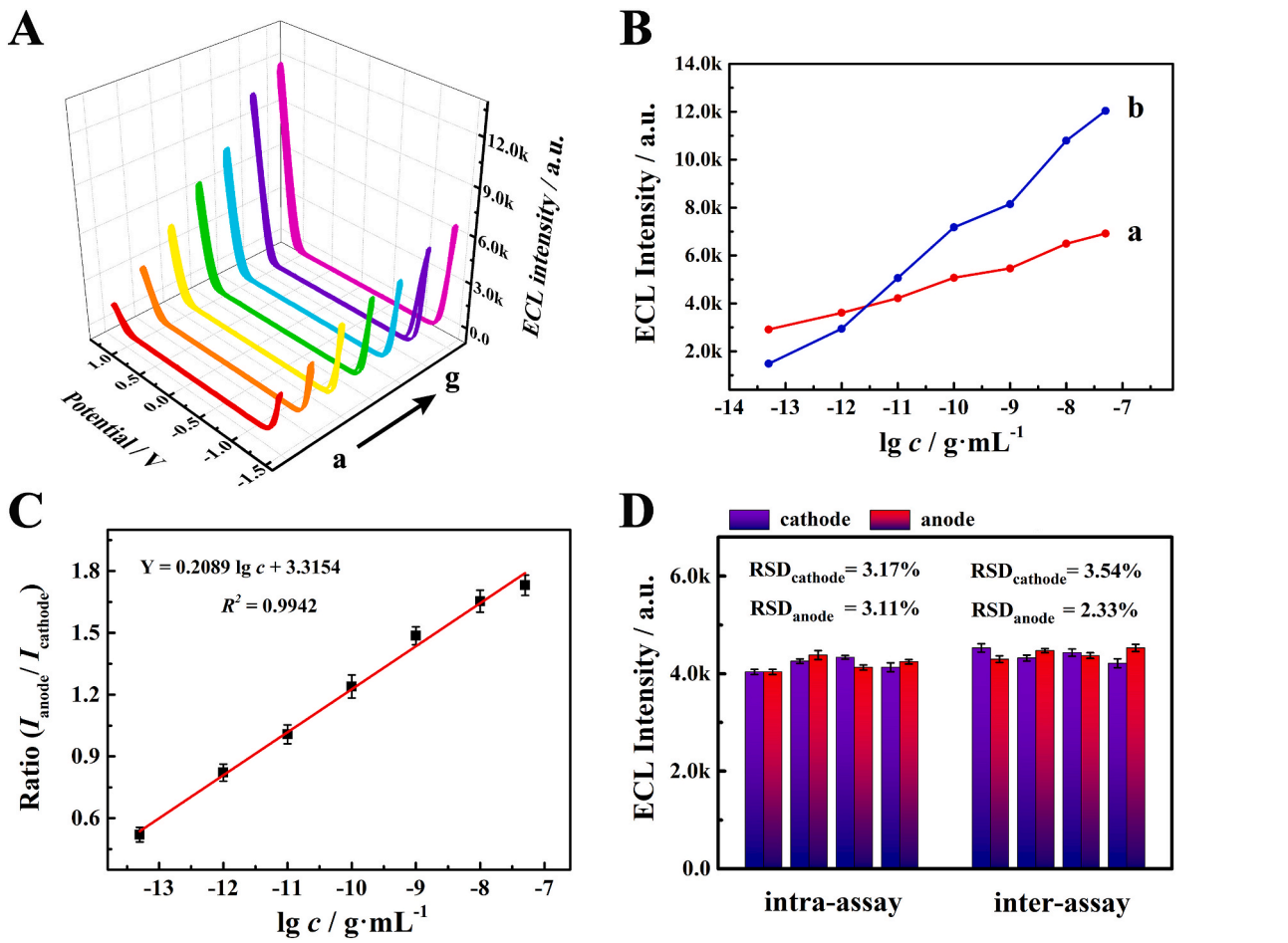

Fig. 4. (A) ECL responses of the immunosensor towards different concentrations of Aβ from (a) to (g): 50 fg/mL, 1.0 pg/mL, 10 pg/mL, 100 pg/mL, 1.0 ng/mL, 10 ng/mL, and 50 ng/mL. (B) Change in $I_{cathode}$ (curve a) and I_{anode} (curve b) with the logarithm of Aβ concentration. (C) Linear curve for Aβ. (D) Intra-assay and inter-assay of the biosensor with 10 pg/mL Aβ. Detection solution: 0.10 M PBS (pH 7.4) containing 5.0 mM $K_2S_2O_8$; scanning rate: 300 mV/s; voltage for photomultiplier: 800 V; scanning potential range: −1.5 V ~ +1.2 V.

respectively, and the two emissions had the same maximum emission wavelength of 706 nm, which was consistent with the cathodic maximum emission wavelength of CdTe QDs alone. The same maximum emission wavelength from the cathode and anode revealed that the anodic emission from CdTe QDs could be mediated by BP nanosheet and two emissions were derived from CdTe QDs. Meanwhile, it is shown that BP nanosheet also has a significant enhancement effect on cathodic emission through comparing the cathodic ECL intensities of CdTe QDs/GCE and BP-CdTe QDs/GCE. This improvement may be attributed to the following fact. The large specific surface area of BP nanosheet enabled CdTe QDs to achieve a high loading on its surface, furthermore, the high charge carrier mobility of BP nanosheet significantly improved the electron transport at the electrode interface (Zhao et al., 2021).

The interference between the two co-reactants DEDA and $K_2S_2O_8$ was explored using BP-CdTe QDs modified GCE and Fig. 2D depicts the corresponding results. The BP-CdTe QDs modified GCE showed relatively weak anodic (1116 a.u.) and cathodic (3721 a.u.) emissions without DEDA and $K_2S_2O_8$ in PBS (curve a). In the presence of 5.0 mM DEDA alone in PBS (curve b), the anodic emission was enhanced (2803 a.u.) due to DEDA as the anodic co-reactant of BP-CdTe QDs, while the cathodic emission remained almost unchanged. In the presence of 5.0 mM $K_2S_2O_8$ alone in PBS (curve c), the cathodic ECL emission was amplified to 5776 a.u. while the anodic emission was same as the anodic emission in curve a, indicating that the anodic and cathodic co-reactants would not interfere with each other.

Additionally, the promoting effect of TiO_2 NSs on two emissions from BP-CdTe QDs was explored using the modified GCE with both BP-CdTe QDs and TiO_2 NSs. As seen, relatively weak two emissions were detected at TiO_2 NSs/BP-CdTe QDs/GCE without DEDA and $K_2S_2O_8$ in PBS (Fig. 2D, curve d), which were almost equivalent to those without TiO_2 NSs (Fig. 2D, curve a). As expectedly, when DEDA (5.0 mM) and $K_2S_2O_8$ (5.0 mM) were present in PBS (Fig. 2D, curve e), two remarkable ECL emissions were produced, and the ECL intensities from the cathode and anode were 9088 a.u. and 11466 a.u., respectively. In addition, the ECL responses of TiO_2 NSs/GCE and bare GCE were further investigated. The results verified that TiO_2 NSs didn't act as luminophor in our ECL system, and the corresponding figures (Fig. S2) and descriptions were presented in Supplementary Material. The above results confirmed that TiO_2 NSs can act as the dual-function co-reaction accelerator to simultaneously modulate the dual-emissions of BP-CdTe QDs.

The cathodic and anodic ECL mechanisms have been explored in Fig. 3. The anodic ECL process without TiO_2 NSs is depicted in Fig. 3A (the left of Fig. 3A). The CdTe QDs and N, N-diethylethylenediamine (DEDA) lose electrons at the electrode interface to generate CdTe QDs$^{\bullet+}$ and DEDA$^{\bullet+}$, respectively. DEDA$^{\bullet+}$ is further deprotonated and transformed into DEDA$^{\bullet}$. Then, CdTe QDs* was formed through electron transfer between CdTe QDs$^{\bullet+}$ and DEDA$^{\bullet}$, resulting in the anodic ECL emission. When TiO_2 NSs were introduced, the anodic ECL emission would be enhanced as TiO_2 NSs would promote the formation of DEDA$^{\bullet+}$ radical, as depicted in the right of Fig. 3A. Fig. 3B depicts the cathodic ECL process. In the absence of TiO_2 NSs (the left of Fig. 3B), CdTe QDs underwent an electro-reduction reaction to obtain CdTe

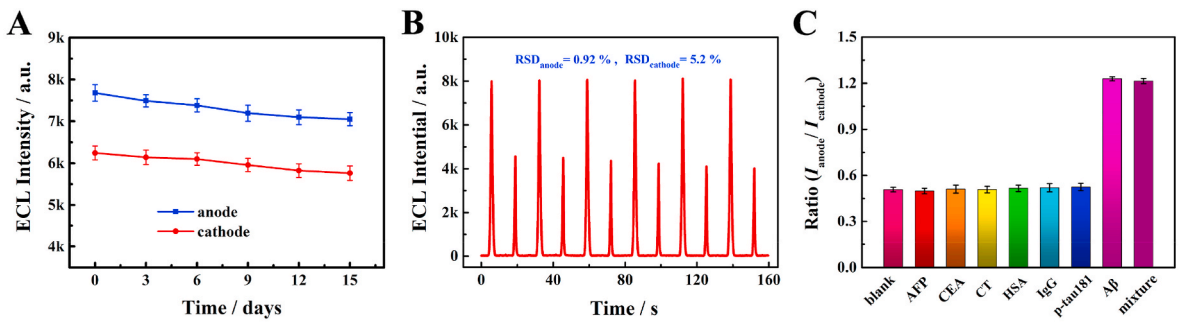

Fig. 5. Storage stability (A) and operational stability (B) of the biosensor with 100 pg/mL Aβ; (C) ECL responses of the immunosensor to blank sample, 1.0 ng/mL AFP, 1.0 ng/mL CEA, 1.0 ng/mL CT, 1.0 ng/mL HAS, 1.0 ng/mL IgG, 1.0 ng/mL p-tau181, 100 pg/mL Aβ and the mixture of previous species. Detection solution: 0.10 M PBS (pH 7.4) containing 5.0 mM $K_2S_2O_8$; scanning rate: 300 mV/s; voltage for photomultiplier: 800 V; scanning potential range: −1.5 V ~ +1.2 V.

$QDs^{\bullet-}$. Similarly, $S_2O_8^{2-}$ was electro-reduced to generate SO_4^{2-} and $SO_4^{\bullet-}$, where $SO_4^{\bullet-}$ could react with CdTe $QDs^{\bullet-}$ to generate CdTe QDs*, resulting the cathodic ECL emission. When TiO_2 NSs were introduced in the cathodic ECL process, they acted as the co-reaction accelerator of $S_2O_8^{2-}$ to amplify cathodic ECL emission by promoting the generation of $SO_4^{\bullet-}$ (the right of Fig. 3B).

3.3. Characterization of biosensor assembly

The assembly of ECL biosensor was characterized using cyclic voltammetry (CV) and electrochemical impedance spectroscopy (EIS), which were performed in 5.0 mM $[Fe(CN)_6]^{3-/4-}$ solution. Fig. S1A depicts the CV results. The bare GCE exhibited a couple of quasi-reversible redox peaks (curve a). When nafion and BP-CdTe QDs were modified on the electrode surface, the peak currents decreased remarkably, which was due to nafion hindering the electron transfer on the electrode surface (curve b). After anti-$A\beta_1$ was captured on the modified electrode (curve c), the oxidation and reduction peak currents further decreased since the protein blocked the electron transfer. With the successive incubation of BSA and Aβ on the modified electrode, the peak currents continued to decrease due to poor conductivity of proteins, and the results were plotted in curve d and curve e, respectively.

The EIS results at each modification stage are depicted in Fig. S1B. Compared with the bare GCE (curve a), the impedance value of BP-CdTe and nafion modified GCE (curve b) increased obviously owing to nafion hindering the electron transfer on the electrode surface. With the successive incubation of anti-$A\beta_1$, BSA, and Aβ on the modified electrode, the impedance values continued to increase due to poor conductivity of proteins, and the results are plotted as curve c, curve d and curve e, respectively. The results of CV and EIS showed the successful construction of ECL biosensor.

3.4. Optimization of experimental conditions

The optimizations of pH and incubation time have been explored, and the results are shown in Fig. S3. As depicted in Fig. S3A, with increasing pH of PBS from 5.0 to 9.0, both the anodic signal intensity (I_{anode}) and cathodic signal intensity ($I_{cathode}$) increased gradually, and the maximum ratio ($I_{anode}/I_{cathode}$) was obtained at pH 7.4 (Fig. S3B). Thus, pH 7.4 was selected as the optimal pH of PBS.

The incubation time of secondary antibody composites was further optimized. As shown in Fig. S3C, the anodic ECL emission intensity (I_{anode}) increased gradually with increasing the incubation time from 30 to 120 min, and reached relative stability after 120 min. Meanwhile, the cathodic ECL intensity ($I_{cathode}$) exhibited a gradually increasing trend with increasing the incubation time from 30 to 90 min, and reached relative stability after 90 min. Significantly, the maximum ratio ($I_{anode}/I_{cathode}$) (Fig. S3D) was obtained when the incubation time was 120 min. Thus 120 min was chosen as the optimal incubation time of secondary antibody composites.

3.5. Performance of biosensor

Under optimal experiment conditions, the quantitative analysis of Aβ was explored in the presence of 5.0 mM $K_2S_2O_8$ in PBS (0.10 M, pH 7.4) using the immunosensor and Fig. 4 depicts the results. When Aβ concentrations went from 50 fg/mL to 50 ng/mL, two ECL emissions gradually increased (Fig. 4A and B). The reasons were explained as follows. An increase in the concentration of the target Aβ led to an increase in the amount of the secondary antibody composites anti-$A\beta_2$-DEDA-Pt@TiO_2 NSs incubated on the electrode, and the amount of DEDA and TiO_2 NSs also increased. The increase in cathodic signal was attributed to the co-reaction accelerator TiO_2 NSs, which can interact with cathodic co-reactant $S_2O_8^{2-}$ in PBS to enhance the emission. The increase in anodic signal was attributed to an increase in the amount of co-reactant DEDA captured at the electrode, as well as an increase in the amount of co-reaction accelerator TiO_2 NSs on the electrode. A good linear relationship was detected between the ratio of anodic signal intensity (I_{anode}) to cathodic signal intensity ($I_{cathode}$) and the logarithm of Aβ concentration (lg *c*) (Fig. 4C). The linear range went from 50 fg/mL to 50 ng/mL and the detection limit was 21 fg/mL (S/N = 3). The regression equation was Y = 0.2089 lg *c*+3.3154 and the square of correlation coefficient was 0.9942, where Y referred to the ratio ($I_{anode}/I_{cathode}$). As shown in Table S1, compared to the existing Aβ detection methods, the constructed immunosensor provided a superior ECL platform for Aβ quantification.

The reproducibility of this biosensor has been evaluated by the intra-assay and inter-assay. For the intra-assay, the four biosensors were prepared using four different GCE (Φ = 4 mm) through the same modification process, and their ECL responses towards 10 pg/mL Aβ were further measured under the same test conditions, including the same operator, the same operation procedure, the same environment and instruments, and the same detection solution. As seen in Fig. 4D, the ECL responses of four biosensors to 10 pg/mL Aβ were nearly identical, and the relative standard deviations (RSD) were 3.17% and 3.11% for the cathodic and anodic ECL signals, respectively. For the inter-assay, the four biosensors were constructed using the same GEC in different batches through the same modification process, and their ECL responses to 10 pg/mL Aβ were further detected under the same test conditions. As depicted in Fig. 4D, no significant change in response was observed, and RSD were 3.54% and 2.33% for the cathodic and anodic ECL signals, respectively. An acceptable RSD for the intra-assay and inter-assay indicated a good reproducibility of our prepared biosensor.

The storage stability of the ECL biosensor with 100 pg/mL Aβ has been investigated by reserving the biosensor at 4 °C for 15 days and taking it out every three days for ECL measurement under the same test conditions. As seen from Fig. 5A, the anodic and cathodic ECL signals could maintain about 91.8% and 92.3% of their original responses after

Table 1
Recovery test in human serum sample.

Sample	Found in serum	Added	Total found [a]	Recovery (%)	RSD (%)
1	0.47 pg/mL	10.0 pg/mL	10.1 ± 0.4 pg/mL	96.3	4.0
2		100 pg/mL	96.7 ± 3.5 pg/mL	96.2	3.6
3		1.00 ng/mL	1.05 ± 0.04 ng/mL	105	3.8
4		10.0 ng/mL	9.72 ± 0.47 pg/mL	97.2	4.8

[a] Average of three determinations ± SD, $n = 3$.

15 days, respectively. In addition, the operational stability of the ECL biosensor was also investigated by continuous cyclic scanning. As shown in Fig. 5B, the ECL responses to 1.0 ng/mL Aβ were hardly changed, and the RSD of anodic and cathodic signals were 0.92% and 5.2%, respectively. The above results indicated that the fabricated immunosensor has an acceptable stability.

The selectivity was also evaluated with carcinoembryonic antigen (CEA), calcitonin (CT), alpha fetoprotein (AFP), human serum albumin (HSA), immunoglobulin G (IgG) and phosphorylated tau181 (p-tau181) protein as possible interfering substances, and their effects are depicted in Fig. 5C. As seen, AFP (1.0 ng/mL), CEA (1.0 ng/mL), CT (1.0 ng/mL), HSA (1.0 ng/mL), IgG (1.0 ng/mL) and p-tau181 (1.0 ng/mL) had almost the same response value as the blank. In the case of the target Aβ (100 pg/mL) alone and the mixture of the target Aβ and all of these interferences, obvious ECL responses were observed, furthermore nearly identical enhancements were obtained, indicating that the fabricated immunosensor had a favorable selectivity.

3.6. Analysis of real serum samples

To examine the practicability of the constructed immunosensor, the recovery experiments were carried out in serum samples by standard addition method. Firstly, the content of Aβ in 50-fold dilution of normal human serum was evaluated using our constructed immunosensor, and 0.47 pg/mL of Aβ was detected. After the several concentrations of standard Aβ samples were added in 50-fold diluted human serum, respectively, the total Aβ concentrations in human serum samples were measured by our constructed immunosensor. Table 1 presents the corresponding results. The recoveries of Aβ in four samples were 96.3%, 96.2%, 105% and 97.2%, and the corresponding RSD were 4.0%, 3.6%, 3.8% and 4.8%, respectively, indicating that the fabricated immunosensor was practicable for the determination of Aβ in clinical analysis.

4. Conclusion

This work developed a novel single-luminophor-based ECL ratiometric immunosensor using dual-emitting BP-CdTe QDs coupled with the dual-function moderator TiO_2 NSs. DEDA and $S_2O_8^{2-}$ served as the anodic and cathodic co-reactants, and TiO_2 NSs could serve as the co-reaction accelerator to simultaneously enhance two emissions. Based on the different increasing trends of the two signals, a sensitive ratio detection of target Aβ was achieved. Benefiting from the unique character of BP-CdTe QDs and TiO_2 NSs, their integration provided a conspicuous single-luminophor-based ECL ratio platform for various biomarkers in the clinical diagnosis and biomedicine detection.

CRediT authorship contribution statement

Jinwen Zhao: Conceptualization, Data curation, Formal analysis, Investigation, Writing – original draft, Writing – review & editing. **Yuting Zhou:** Data curation, Writing – original draft, Investigation. **Ying He:** Conceptualization, Supervision. **Xingrong Tan:** Conceptualization, Supervision. **Ruo Yuan:** Funding acquisition, Resources, Supervision. **Shihong Chen:** Funding acquisition, Resources, Project administration, Writing – review & editing.

Declaration of competing interest

The authors declare that they have no known competing financial interests or personal relationships that could have appeared to influence the work reported in this paper.

Acknowledgments

This work was supported by NNSF of China (21775122, 21775124), and Natural Science Foundation of Chongqing City (cstc2018jcyjAX0693, cstc2021jcyj-msxmX0968), China.

Appendix A. Supplementary data

Supplementary data to this article can be found online at https://doi.org/10.1016/j.bios.2022.114420.

References

Cao, S., Luo, Q., Li, Y., Liang, R., Qiu, J., 2020. Chem. Commun. 56, 5625–5628.
Chen, H., Li, W., Wang, Q., Jin, X., Nie, Z., Yao, S., 2016. Electrochim. Acta 214, 94–102.
Chen, H., Liu, X., Yin, C., Li, W., Qin, X., Chen, C., 2019. Analyst 144, 5215–5222.
Du, Y., Xue, J., Sun, X., Wu, D., Liu, X., Ju, H., Yang, L., Wei, Q., 2020. Anal. Chem. 92, 8472–8479.
Gao, X., Fu, K., Fu, L., Wang, H., Zhang, B., Zou, G., 2020. Biosens. Bioelectron. 150, 111880.
Hao, Q., Xu, Q., Niu, S., Ding, C., Luo, X., 2021. Anal. Chem. 93, 10679–10687.
He, Y., Hu, F., Zhao, J., Yang, G., Zhang, Y., Chen, S., Yuan, R., 2021. Anal. Chem. 93, 8783–8790.
Hu, L., Wu, Y., Xu, M., Gu, W., Zhu, C., 2020. Chem. Commun. 56, 10989–10999.
Huo, X.L., Lu, H.J., Xu, J.J., Zhou, H., Chen, H.Y., 2019. J. Mater. Chem. B 7, 6469–6475.
Lei, Y., Huang, W., Zhao, M., Chai, Y., Yuan, R., Zhuo, Y., 2015. Anal. Chem. 87, 7787–7794.
Lu, Y., Ke, H., Wang, Y., Zhang, Y., Li, H., Huang, C., Jia, N., 2020. Biosens. Bioelectron. 170, 112664.
Ma, J., Wang, W., Li, Y., Lu, Z., Tan, X., Han, H., 2021. Anal. Chem. 93, 2090–2096.
Pan, D., Chen, K., Zhou, Q., Zhao, J., Xue, H., Zhang, Y., Shen, Y., 2019. Biosens. Bioelectron. 131, 178–184.
Shang, L., Wang, X., Zhang, W., Jia, L., Ma, R., Jia, W., Wang, H., 2020. Sensor. Actuator. B Chem. 325, 128776.
Shang, Q., Zhou, Z., Shen, Y., Zhang, Y., Li, Y., Liu, S., Zhang, Y., 2015. ACS Appl. Mater. Interfaces 7, 23672–23678.
Wang, C., Zhang, N., Li, Y., Yang, L., Wei, D., Yan, T., Ju, H., Du, B., Wei, Q., 2019a. Sensor. Actuator. B Chem. 291, 319–328.
Wang, H., 2021. Anal. Bioanal. Chem. 413, 4119–4135.
Wang, J., Haghighatbin, M.A., Shen, W., Mi, L., Cui, H., 2020. Anal. Chem. 92, 7062–7070.
Wang, Y., Shan, D., Wu, G., Wang, H., Ru, F., Zhang, X., Li, L., Qian, Y., Lu, X., 2018. Biosens. Bioelectron. 106, 64–70.
Wang, Y., Zhang, Y., Sha, H., Xiong, X., Jia, N., 2019b. ACS Appl. Mater. Interfaces 11, 36299–36306.
Xie, Y., Zhang, M., Bin, Q., Xie, S., Guo, L., Cheng, F., Lv, W., 2020. Biosens. Bioelectron. 150, 111949.
Xue, J., Yang, L., Wang, H., Yan, T., Fan, D., Feng, R., Du, B., Wei, Q., Ju, H., 2019. Biosens. Bioelectron. 133, 192–198.
Yang, G., He, Y., Zhao, J., Chen, S., Yuan, R., 2021. Sensor. Actuator. B Chem. 341, 130008.
Yu, L., Li, M., Kang, Q., Fu, L., Zou, G., Shen, D., 2021. Biosens. Bioelectron. 176, 112934.
Zeng, W., Liao, N., Lei, Y., Zhao, J., Chai, Y., Yuan, R., Zhuo, Y., 2018. Biosens. Bioelectron. 100, 490–496.
Zhang, G., Chai, H., Tian, M., Zhu, S., Qu, L., Zhang, X., 2020. Anal. Chem. 92, 7354–7362.
Zhang, H., Xu, J., Chen, H., 2013. Anal. Chem. 85, 5321–5325.
Zhao, J., He, Y., Tan, K., Yang, J., Chen, S., Yuan, R., 2021. Anal. Chem. 93, 12400–12408.
Zhou, X., Zhang, W., Wang, Z., Han, J., Xie, G., Chen, S., 2020. Biosens. Bioelectron. 148, 111795.